PROCEEDINGS OF THE ROYAL SOCIETY A MATHEMATICAL, PHYSICAL & ENGINEERING SCIENCES

Diffusion of curvature on a sheared semi-infinite film

Journal:	*Proceedings A*
Manuscript ID:	Draft
Article Type:	Research
Date Submitted by the Author:	n/a
Complete List of Authors:	Satomi, Ryo; University of Manchester, CEAS Grassia, Paul; University of Manchester, School of Chemical Engineering and Analytical Science Cox, Simon; Aberystwyth University, IMAPS Mishuris, Gennady; Aberystwyth University, IMAPS Lue, Leo; University of Strathclyde, Chemical and Process Engineering
Subject:	Applied mathematics < MATHEMATICS, Computer modelling and simulation < COMPUTER SCIENCE, Mathematical modelling < MATHEMATICS
Keywords:	Viscous froth model, Curvature-driven motion, Diffusion of curvature, Foam rheology, Surface Evolver, Asymptotic analysis

Diffusion of curvature on a sheared semi-infinite film

Ryo Satomi, Paul Grassia
CEAS, The Mill, The University of Manchester,
Oxford Road, Manchester M13 9PL, UK
ryo.satomi@gmail.com, paul.grassia@manchester.ac.uk

Simon Cox, Gennady Mishuris
IMAPS, Aberystwyth University, Aberystwyth, Ceredigion SY23 3BZ, UK
foams@aber.ac.uk, ggm@aber.ac.uk

Leo Lue
Chemical and Process Engineering, University of Strathclyde
James Weir Building, 75 Montrose Street, Glasgow G1 IXJ, UK
leo.lue@strath.ac.uk

Abstract

The viscous froth model is used to study the evolution of a long soap film which is sheared by moving its end point at a constant velocity in a direction perpendicular to the initial film orientation. Film elements are thereby set into motion as a result of the shear, but these moving film elements then experience viscous dissipation. This simple scenario enables analysis of the transport of curvature along the film, which is important in foam rheology, in particular for energy-relaxing 'topological transformations'. Curvature is shown to be transported diffusively along films, with an effective diffusivity scaling as the ratio of film tension to the viscous drag coefficient. Computed (finite-length) film shapes at different times are found to approximate well to the semi-infinite film and are observed to collapse with distances rescaled by the square root of time. The tangent to the film at the end point reorients so as to make a very small angle with the line along which the film end point is dragged, and this angle decays roughly exponentially in time. The numerical results are described in terms of a simple asymptotic solution corresponding to an infinite film that initially contains a right angled corner.

Keywords: Viscous froth model, Curvature-driven motion, Diffusion of curvature, Foam rheology, Surface Evolver, Asymptotic analysis

1 Introduction

Flowing foams occur in a variety of applications such as oil recovery, froth flotation and microfluidics, making them of research interest [1, 2, 3]. A detailed understanding of foam rheology requires description of foam structure on the bubble scale. This has been achieved in the quasistatic slow flowing limit, for structures in mechanical equilibrium (at a minimal energy state [2]). In faster foam flows however, the structure departs from quasistatic mechanical equilibrium and dissipative processes become significant [4].

Various models have been developed to simulate the rheology of foams, such as the bubble model [5], the vertex model [6] and the viscous froth model [4, 7]. Among such models, the viscous froth model has proven to be a powerful tool to simulate the rheology of dry foams, predicting realistic bubble shapes and agreeing with experimental results for "2-dimensional" foam flows in channels i.e. foam monolayers confined between upper and lower plates [7, 8, 9]. In this geometry, a foam film can be represented mathematically by a curve in the "2-dimensional" plane. The viscous froth model [3, 7, 8, 9, 10, 11, 12, 13] applied to such "2-dimensional" systems is based on a force balance between the pressure difference across the two sides of the film (ΔP), the film tensions (γ) and the viscous drag on each film element (the drag being associated with moving the films over the confining upper and lower plates):

$$\lambda \boldsymbol{v} = \Delta P \boldsymbol{n} - c\gamma \boldsymbol{n} \tag{1}$$

where λ is the viscous drag coefficient per unit length of film, $\boldsymbol{v}$ is the velocity of a film element, $\boldsymbol{n}$ is the unit vector normal to the film element, and c is the "2-dimensional" film curvature.

One particularly attractive feature of the viscous froth model over others is its capability to account for film curvatures which are not simply arcs of circles. This feature is not strictly necessary when simulating foams which are slowly sheared, i.e. in systems with low capillary number (the ratio of the imposed foam deformation rate and the relaxation rate), as the viscous term in equation 1 would then be negligibly small, reducing the equation to the Young-Laplace law and thus the curvature of each film would simply be well represented by a constant $\Delta P/\gamma$. As velocities increase however, curvature deviates from this value and tends

to vary with position.

We motivate this work by considering a periodic regular hexagonal array, the hexagonal honeycomb structure. The pressures in every bubble are identical and thus films in the slowly sheared limit do not have any curvature. However, upon fast shear (high capillary number), the viscosity is important and curvature becomes spatially non-uniform, complicating the shape of the films even in the case of the hexagonal honeycomb structure [4, 13, 14].

Elongated bubbles then arise [15] because bubble neighbour exchange transformations, so-called T1 topological transformations, which tend to relax film energy, are suppressed. Films are required to meet threefold at vertices, and a T1 is produced by moving two vertices together until the point at which they collide. The velocity of a vertex is determined by the curvatures of the adjoining films [13]. In the hexagonal honeycomb case (with equal pressures in all bubbles) this can be expressed as[1]:

$$\boldsymbol{v}_v = -\frac{2}{3}\frac{\gamma}{\lambda}\Sigma_{i=1}^{3} c_i(0)\boldsymbol{n}_i \tag{2}$$

where $\boldsymbol{v}_v$ is the velocity of the vertex, $c_i(0)$ is the curvature of film i at the vertex ($i = 1, 2, 3$), and $\boldsymbol{n}_i$ is the normal to the film i.

In the hexagonal honeycomb case, for any finite λ, it is clearly necessary to have film curvature in order to set vertices in motion (and ultimately to induce a T1). Hence a relevant question is to ask how rapidly curvature can be transported along foam films in a sheared foam, since curvature is injected into the film by the shear, but the T1 relies on transport of the curvature along the film. The purpose of this paper is therefore to consider transport of curvature for a highly simplified yet generic case, the shearing of a single semi-infinite film (see Section 2). We will compare computed simulation data (Section 3) with a late time asymptotic solution (Section 4). The asymptotic solution can be analysed further to gain insights into the behaviour of the system (Sections 5–6). Conclusions are offered in Section 7.

[1]Note that according to equation 2, only in the limit as $\lambda \to 0$ does it become possible to displace the vertex without curvature. For a hexagonal foam, this corresponds to the 'slow displacement' quasi-static limit of Princen [16].

2 Description of the system to be studied

Consider a semi-infinite foam film that is initially straight, with no pressure drop across it. One of its endpoints is then moved perpendicular to the film orientation with a velocity v_{shear} (see figure 1).

Then, since γ/λ has the units of a diffusivity D, it follows that D/v_{shear} is a length scale and D/v_{shear}^2 is a time scale[2]. We make lengths and times dimensionless on these scales and curvature dimensionless on the scale v_{shear}/D.

Since there is no imposed pressure difference, equation 1 then becomes

$$\left(\frac{\mathrm{d}\boldsymbol{X}}{\mathrm{d}t}\right)_{\Theta} = -\kappa\boldsymbol{n}, \tag{3}$$

where $\boldsymbol{X}$ is the dimensionless location of a film element, t is the dimensionless time, Θ labels a material point, κ is the dimensionless curvature and $\boldsymbol{n}$ is the unit vector normal to the film surface. This then corresponds to motion by mean curvature [19], a model which has also been used in a different physical context to describe grain growth [13, 20].

For dimensionless times $t \ll 1$, it turns out that the film turns through a very small angle over its entire length. However for times $t \geq O(1)$ the film turns through an appreciable angle and the end point of the film meets the horizontal boundary in figure 1 at an angle significantly different from $\pi/2$. In fact the meeting angle decays very rapidly as t increases – a phenomenon which we will investigate later. One of the reasons for analysing the behaviour of this angle is that (in our dimensionless system) its cosine represents the force that must be applied to the film endpoint to drag the film along. This is also (again in our dimensionless system) the rate of working by the dragging force, some of that work being stored as an increased film length, and some of it being dissipated viscously.

There is a well-known solution in the literature for a *finite* film dragged at both ends, known as the Mullins finger or the grim reaper [13, 20]. Consider a film of initial length L the end points of which are both pulled at velocity v_{pull} (perpendicular to the initial orientation of

[2]Values of λ can be quite difficult to determine and are sensitive to details of a particular experiment [17, 18], but reference [8] has quoted a value 290 kg m^{-2} s^{-1}. Taking a film tension γ of say 29×10^{-3} N m^{-1}, gives diffusivity D of the order of 10^{-4} m^2 s^{-1}. If the film end point is dragged at a velocity v_{shear} of 0.1 m s^{-1}, the characteristic length scale becomes 10^{-3} m and and the characteristic time scale would be 10^{-2} s.

the film) such that the separation of the end points remains unchanged. Making the system dimensionless on scales as above, the dimensionless initial length is

$$l = \frac{Lv_{pull}}{D} \tag{4}$$

and the dimensionless velocity of the end points is unity. The final state depends on the initial length. If $l < \pi$, it is a finite segment of reaper propagating at unit velocity (see figure 2). The angle through which the reaper turns between the symmetry point at its tail and the dragged end point is less than $\pi/2$. On the other hand, if $l > \pi$, the solution is an infinitely long reaper propagating at velocity $\pi/l < 1$ (again see figure 2). The reaper turns through $\pi/2$ between the symmetry point at its tail and the end point. The dragged end points move at unit velocity (hence the reaper becomes stretched infinitely long) in the direction of propagation.

The present case of a dragged *semi-infinite* film however is rather different. The curved region of the film is not confined to a fixed lateral distance but rather the curvature extends over longer and longer lateral distances as time evolves. This means the evolution slows down. The long time asymptotic state of the semi-infinite film therefore cannot be mapped on to a reaper. There is however another solution to which it corresponds. This is the case of an infinite film that initially turns through a sharp right angle corner. This is sketched in figure 3 (and is analogous to some solutions with initial sharp corners considered by Weaire and McMurry [13]). Surface tension acts to smooth out the corner and the film immediately evolves into a curve. This system (of a film that turns through a right angle) becomes the same as the sheared semi-infinite film provided that the extent of the region over which the curvature is distributed at any given time t, is considerably less than the distance that the end point of the sheared semi-infinite film has been moved; thus the end point of the semi-infinite film is extremely far from the curved region. The end point's exact location is no longer relevant to determining the evolution of that curved region – the end point has in effect moved an arbitrarily far distance away from that region. We shall return to consider this long time asymptotic solution in due course, but first we consider some (numerical) simulation data at finite time.

3 Simulation of the dragged film

We have simulated the dragged film numerically using Surface Evolver [21]. We cannot of course represent a semi-infinite film numerically, so we have chosen long finite films of length 40, 100, and 200 each discretised into segments (with individual segment lengths ranging between 0.01 and 0.05 units). *Both* ends of the film are displaced with unit velocity, and we used a time step of 10^{-4} units to evolve the film shape. The above numerical simulation procedure actually corresponds to the start up of the *reaper* problem discussed in Section 2.

At sufficiently early times (see figure 4) there is a straight (vertical) central section of the film which has not moved significantly. At these early times, either end of the finite film will be a good representation of the semi-infinite case. The maximum amount of time for which we can use the finite film to represent the semi-infinite one increases as the film length increases. For instance, for a film of initial length 40 we could simulate out to time 8 units before the film midpoint was moved by a distance of 10^{-6}. However for a film of initial length 100 we could simulate out to time 45 before the film midpoint moved by the same amount, whereas for initial length 200 we could simulate all the way out to time 180. These simulations however also become much more expensive as the film length increases – for initial length 40 units, the run time was 15 minutes (on an i3 CPU, 3.10 GHz), whereas for initial length 200 units, the run time was 48 hours.

Figure 5 shows data for the curved film shapes at times t equal to 40, 70 and 120 for the case of an initial film length of 200. The film is drawn on a Cartesian coordinate domain, and is assumed initially to be at a coordinate location $x = 0$ whilst covering $-200 \leq y \leq 0$. On the figure, we only plot the domain $-100 \leq y \leq 0$ and $x \geq 0$, so we are only plotting half the film shape, it being symmetric about the line $y = -100$.

Our aim is to understand how far curvature is transported along the film as a function of time, since (as was mentioned in Section 1) film curvature leads (in the case of a foam, as opposed to that of just a single film) to vertex motion, and vertex motion is a pre-requisite of any energy relaxing topological transformation in foam. Figure 5 shows (unsurprisingly) that at longer times curvature has been transported over a longer lateral distance of film (i.e. transported over a greater distance along the y-axis). There are however some additional

interesting features in the figure.

Even though the ultimate source of the curvature is the imposed motion of the top boundary (which at time t has displaced to $x = t$), the maximum of the curvature does not occur at that topmost point. Indeed sections of the $t = 70$ and $t = 120$ curves are almost completely aligned with the x-axis from $x = t$ (i.e. the film endpoint) down to about $x \sim 40$. The region of maximum curvature is much further back at smaller x values: the figure also shows a zoomed view of that region. In that zoomed view, we see at time $t = 40$, that the shape of the film is qualitatively different either side of the quadrant 'bisector' $\theta = -\pi/4$, i.e. there is asymmetry between polar coordinate angles $-\pi/2 \leq \theta \leq -\pi/4$ and angles $-\pi/4 \leq \theta \leq 0$ (contrast figure 3). When $t = 40$, the film tends to be more curved for $-\pi/2 \leq \theta \leq -\pi/4$, but exhibits a long rather flattened section for $-\pi/4 \leq \theta \leq 0$. As curvature is needed to drive motion here, the flattened section barely moves (e.g. it displaces comparatively little between times $t = 40$ and $t = 70$). By $t = 70$ however the flattened section has been eroded, and so these film points are now able to move again. The asymmetry between the polar angles $-\pi/2 \leq \theta \leq -\pi/4$ and $-\pi/4 \leq \theta \leq 0$ is much reduced by $t = 70$, a tendency which increases towards $t = 120$.

Figure 6 shows data for rescaled film positions – rescaling distances by $t^{1/2}$ (on the grounds that diffusive problems often exhibit this type of scaling). These collapse together reasonably well – although, if we subdivide the solution quadrant into two halves, this collapse tends to be much better for polar angles $-\pi/2 \leq \theta \leq -\pi/4$ than for polar angles $-\pi/4 \leq \theta \leq 0$. Given the (above noted) asymmetry of the $t = 40$ film in these two angular domains, contrasted with the near symmetry of the $t = 120$ film, we do not expect to obtain equally good collapse in both domains. Nevertheless figure 6 is indicating that curvature is transported out to a lateral distance (i.e. out to a distance $|y|$ in the figure) of order $t^{1/2}$ – this is a result we wish to understand (and we return to it shortly in Section 4).

Figure 7 shows data for the angle ψ at which the film meets the line along which its end point is dragged (see also the definition sketch figure 1). This is initially $\pi/2$ – the film meets the line at right angles. Very rapidly however the film reorients – at its end point it becomes nearly parallel to the line along which its end point is dragged.

How rapidly that angle decays to zero in the long time limit is behaviour that we would like to analyse. The data on figure 7 have been plotted on a log-linear scale, and show a reasonably

straight region on the plot. Thus the angle ψ is decaying roughly exponentially to zero over time. By fitting the decay data over the (arbitrarily chosen) range $10^{-4} \leq \psi \leq 10^{-1}$ to an exponential, the characteristic decay time turns out to be 2.65 units. The fit is poor at early times (since early time data were excluded from the fit) but is also poor in relative terms at very late times (an artifact of the fitting procedure which minimizes the sum of squares of absolute errors, and hence incurs little penalty from relative errors if ψ is small). Nevertheless the notion of an exponential fit is a fair approximation to the data: over the range of ψ mentioned above, the fitting procedure reported rms errors in ψ between the data and the exponential fit of only 5×10^{-4}. The origin of this rapid near-exponential decay for ψ is another feature that we wish to understand.

To summarise, Surface Evolver furnishes us with useful simulation data for understanding the dragged film problem. However to access very long times (and still have a reasonable representation of the semi-infinite film case), requires the use of very long but finite films in the simulation and this becomes expensive numerically. What we seek therefore is to understand the long-time behaviour of the dragged film using an asymptotic approach without relying on simulations – this is the topic of the next section.

4 A late time asymptotic solution

In what follows we compute the similarity solution for the corner in figure 3, which corresponds to the long time asymptotic behaviour of a sheared film. This is clearly a solution that is symmetric under reflection about the bisector of the original corner.

In order to obtain this solution, there are various ways one can parameterise the film. For instance one could parameterise based on material points or based on arc length along the film (see Appendix). Here however, a polar coordinate system $\tilde{r}$ *vs.* θ will be chosen.

Projecting the vector equation 3 onto the radial and angular directions in polar coordinates, one obtains

$$\left(\frac{\mathrm{d}\tilde{r}}{\mathrm{d}t}\right)_{\Theta} = -\kappa n_{\tilde{r}} \tag{5}$$

$$\left(\frac{\mathrm{d}\theta}{\mathrm{d}t}\right)_{\Theta} = -\frac{\kappa n_{\theta}}{\tilde{r}} \tag{6}$$

where $\tilde{r}$ is the radial position, θ is the angular position, and $n_{\tilde{r}}$ and n_θ are the radial and angular components of the normal vector $\boldsymbol{n}$ respectively. Furthermore, the radial position of a film element can be considered to be a function of time and angular position, which itself is a function of time and material point, i.e. $\tilde{r}\left(t, \theta\left(t, \Theta\right)\right)$. Then the following differential equation holds:

$$\left(\frac{\mathrm{d}\tilde{r}}{\mathrm{d}t}\right)_\Theta = \left(\frac{\mathrm{d}\tilde{r}}{\mathrm{d}t}\right)_\theta + \left(\frac{\mathrm{d}\theta}{\mathrm{d}t}\right)_\Theta \frac{\mathrm{d}\tilde{r}}{\mathrm{d}\theta}. \tag{7}$$

Assuming that $\tilde{r}(t,\theta) = a(t)r(\theta)$, where $a(t)$ is a scale factor to be determined and $r(\theta)$ is a rescaled radial position, we deduce:

$$n_{\tilde{r}} = \frac{r}{\sqrt{r^2 + r'^2}} \tag{8}$$

$$n_\theta = -\frac{r'}{\sqrt{r^2 + r'^2}} \tag{9}$$

where r' denotes the first derivative of r with respect to θ. Moreover since the tangent vector is just a rotated version of the normal, and since the curvature is simply the derivative of the tangent with distance along the film projected back onto the normal, we obtain

$$\kappa = \frac{1}{a}K; \tag{10}$$

here[3]

$$K = \frac{r^2 + 2r'^2 - rr''}{\left(r^2 + r'^2\right)^{3/2}} \tag{11}$$

where r' is as above, and r'' is the second derivative of r with respect to θ.

Substituting equations 5, 6 and 10 into equation 7 (and using $\dot{a}$ to denote the derivative of a with respect to time),

$$\dot{a}r - \frac{Kn_\theta}{ar}r' = -\frac{K}{a}n_{\tilde{r}}. \tag{12}$$

From equation 12 it is clear that we should choose $a = \sqrt{t}$ (thereby confirming the diffusive nature of the system), from which it follows that

$$-Kn_{\tilde{r}} = \frac{r}{2} - \frac{Kn_\theta}{r}r'. \tag{13}$$

[3]Note that κ and K turn out to be negative quantities in the particular sign convention we adopt here.

Further substituting from equations 8, 9 and 11 and rearranging gives

$$r'' = \frac{2r^2 + r^4 + 4r'^2 + r^2 r'^2}{2r}. \tag{14}$$

A description $r = r(\theta)$ as in equation 14 is convenient near the symmetry line $\theta = -\pi/4$. However near the asymptote $\theta = 0$, the value of r should tend to infinity and a more convenient description then is $\theta = \theta(r)$; the chain rule gives trivially

$$r' = \theta'^{-1} \tag{15}$$

where θ' is the derivative of θ with respect to r. Further differentiating with respect to r and substituting equations 14 and 15 where appropriate gives

$$\theta'' = -\theta'^3 \frac{2r^2 + r^4 + 4\theta'^{-2} + r^2\theta'^{-2}}{2r}. \tag{16}$$

Equation 14 can be numerically integrated given initial values of r and r', and may be switched to equation 16 at any point to continue integrating. Assuming the shearing takes place in the fourth quadrant (i.e. for $-\pi/2 \leq \theta \leq 0$), the obvious symmetry condition is that $r' = 0$ at $\theta = -\pi/4$. However the value of r at $\theta = -\pi/4$ (which we denote as r_0) must be found by a trial and error shooting procedure, on the basis that θ should tend to zero as r tends to infinity. Results of the numerical integration with varying values of r_0 are given in figure 8. To avoid unnecessary numerical expense, the step size was increased adaptively[4]. As a result, the curves shown in figure 8 could be obtained in under 100 steps.

Clearly, the asymptotic angle between the ends of the film is dependent on r_0. Too large a value of r_0 leads to films which curve too sharply and turn through more than $\pi/4$ between the symmetry point and the asymptote. Conversely, too small a value of r_0 leads to films which curve too little, and turn through too small an angle. From the solutions obtained, $r_0 \approx 1.0445$ gave a film curved by the correct amount, and thus was adopted as the right initial condition

[4]Specifically whilst integrating for θ as a function of r we considered the discrepancy between doing two steps with an integration step size δr and doing one step with an integration step size $2\,\delta r$: if the discrepancy was exceedingly small compared with the change in θ during the step, we considered it safe to increase the step size.

thereafter.

Solutions obtained using this r_0 value have also been plotted on figure 6 and compared with the scaled simulation data. Agreement is imperfect (as might be expected, since the Evolver data were obtained at finite times, rather than in the long-time asymptotic limit). Nevertheless the Evolver data do indicate a tendency to converge towards the asymptotic state.

Returning to the asymptotic solution, as the film approaches the coordinate axes (either the x-axis or the y-axis), the step wise changes in angle become smaller. Since numerical calculations are limited by finite precision, it is preferable to switch eventually to an approximate analytic formula for θ *vs.* r. As r increases and θ' decreases, equation 16 becomes approximately

$$\theta'' \approx -\frac{4+r^2}{2r}\,\theta'. \tag{17}$$

Integrating with respect to r,

$$\theta' \approx \frac{A}{r^2}\exp\left(-\frac{r^2}{4}\right) \tag{18}$$

where A is an integration constant.

In the limit as $r \to \infty$, θ should approach some 'final' value θ_f which should itself be close to zero provided the parameter r_0 has been chosen correctly[5]. At θ close enough to the final angle, θ_f, the value of A can be obtained by fitting the numerical θ' *vs.* r values to equation 18. Then the final angle θ_f can be obtained by integrating equation 18 out to an arbitrarily large r. For consistency we have checked that the A value is insensitive to the choice of angle at which we switch from the numerical integration to the analytical formula, and moreover that the predicted final angle θ_f is close to zero.

Table 1 shows the computed results varying the angle at which the switch to the approximate analytic solution takes place: convergence is obtained provided we switch around $-0.001 \times \pi/2$ or at any other angle closer to zero than that. The analytic solution (i.e. the decay of θ with r) can then be followed for several decades more, down to the point at which θ reaches the neighbourhood of θ_f. Once however θ attains a value close to θ_f, the solution becomes 'unreliable' being sensitive to the fact that our guess for the parameter r_0 was not quite correct

[5]For any given r_0, the value of θ_f is the angle that the curve in figure 8 makes with the x-axis, as x tends to infinity.

(i.e. the film turns through not quite the correct angle along its length, so θ_f is not exactly zero). However the θ_f values reported in table 1 are so tiny that this discrepancy poses no real difficulty.

5 Reorientation of the film end point

In the computed results of Section 3 we saw that the angle ψ at which the film meets the line along which its end point is dragged decays very rapidly with time. Although the asymptotic results of Section 4 deal with an infinite film with an initial right angle corner (rather than a sheared semi-infinite one), we can nevertheless use the asymptotic results to gain insights into the behaviour observed in the semi-infinite case. The dragged end point of the semi-infinite film is displaced a distance $\tilde{r} = t$ (i.e. $r \equiv \tilde{r}/t^{1/2} = t^{1/2}$) away from its original location. Hence we can look at the film orientation at points on the asymptotic solution which are the same distance away from the origin. Unlike in the simulations, these will not be exactly at polar angle $\theta = 0$, but (provided the distance is large) the θ value will be very close to zero. The angle ψ can be evaluated as

$$\psi = \arccos\left(\boldsymbol{t} \cdot \boldsymbol{e_x}\right) \tag{19}$$

where $\boldsymbol{e_x}$ is the Cartesian unit vector and $\boldsymbol{t}$ is the tangent vector

$$\boldsymbol{t} = \frac{\boldsymbol{e_r} + r\theta'\boldsymbol{e_\theta}}{\sqrt{1 + (r\theta')^2}} \tag{20}$$

and $\boldsymbol{e_r}$ and $\boldsymbol{e_\theta}$ are polar unit vectors. Here $\boldsymbol{e_r} \cdot \boldsymbol{e_x} = \cos\theta$ and $\boldsymbol{e_\theta} \cdot \boldsymbol{e_x} = -\sin\theta$. Values for ψ *vs.* t evaluated at $r = t^{1/2}$ according to the above formula and using the asymptotic analysis of Section 4 are plotted in figure 9. As in figure 7, we plot here on a log scale, so that it is clear that ψ actually exhibits very rapid decay, with a near straight line on the plot being indicative of a near-exponential decay.

In the limit where θ is exceedingly close to zero we have

$$\psi \approx \frac{\mathrm{d}y}{\mathrm{d}x} \tag{21}$$

where $y \approx r\theta$ and $x \approx r$. Hence

$$\frac{\mathrm{d}y}{\mathrm{d}x} \approx \frac{\mathrm{d}}{\mathrm{d}r}(r\theta) \approx r\theta' + \theta. \tag{22}$$

We write this as $r\theta' + \theta_f + (\theta - \theta_f)$ where θ' is given by equation 18 and hence

$$\theta_f - \theta = \int_r^\infty \frac{A}{\bar{r}^2} \exp\left(-\frac{\bar{r}^2}{4}\right) \mathrm{d}\bar{r} \tag{23}$$

with $\bar{r}$ a dummy integration variable. Integrating by parts:

$$\begin{aligned} \theta_f - \theta &= \frac{A}{r}\exp\left(-\frac{r^2}{4}\right) - \int_r^\infty \frac{A}{2}\exp\left(-\frac{\bar{r}^2}{4}\right)\mathrm{d}\bar{r} \\ &= r\theta' - \frac{\sqrt{\pi}A}{2}\,\mathrm{erfc}\left(\frac{r}{2}\right) \end{aligned} \tag{24}$$

where equation 18 has been used. Substituting from equations 21 and 22 then gives

$$\psi \approx \theta_f + \frac{\sqrt{\pi}A}{2}\,\mathrm{erfc}\left(\frac{r}{2}\right), \tag{25}$$

and (as alluded to above) we are required to evaluate this at location $r = t^{1/2}$ so that

$$\psi \approx \theta_f + \frac{\sqrt{\pi}A}{2}\,\mathrm{erfc}\left(\frac{t^{1/2}}{2}\right). \tag{26}$$

We are interested here in r and t values which are large compared to unity, but nevertheless such that the complementary error function term is considerably larger than θ_f (otherwise the ψ value we compute is sensitive to the fact that our chosen r_0, as obtained via shooting, gives θ_f values that differ very slightly from zero).

Based on equation 23, we can estimate that $\theta_f - \theta$ will be at most a number on the order of $r^{-3}\exp(-r^2/4)$ and hence is much smaller than $r\theta'$ (found using equation 18) when r is large. It follows that the two terms on the right hand side of equation 24 nearly cancel (since the left hand side of that equation is smaller than the first term on the right). If we are in a regime of r values (as alluded to above) where the complementary error function term is still much larger

than θ_f, it follows that

$$\psi \approx r\theta' \approx \frac{A}{r}\exp\left(-\frac{r^2}{4}\right). \tag{27}$$

Evaluated at $r = t^{1/2}$, this gives

$$\psi \approx \frac{A}{t^{1/2}}\exp\left(-\frac{t}{4}\right), \tag{28}$$

hence the near-exponential decay of ψ observed in figure 9.

The time constant of the exponential decay for ψ for this asymptotic model according to equation 28 is not quite the same as that obtained from the Surface Evolver results (see figure 7), but this is unsurprising given the different θ values at which the angle ψ is evaluated in the two models (at $\theta = 0$ for the numerical Surface Evolver data, but at a small non-zero θ for the asymptotic solution). Moreover the $t^{-1/2}$ prefactor in the formula (equation 28) means the decay is not quite a pure exponential in any case.

6 Movement of material points on a film

Having obtained the shape of the curved film in Section 4, the movement of material points can be tracked: following material points is of interest because, even though shearing a film (as in Section 3) adds new material to the film and increases its overall length, it turns out that film material elements once created, invariably *shrink*. Taking $\mathrm{d}\boldsymbol{X}$ to represent an element of film with length $\mathrm{d}s$, and differentiating the relationship $(\mathrm{d}s)^2 = \mathrm{d}\boldsymbol{X}\cdot\mathrm{d}\boldsymbol{X}$ with respect to time and substituting $\boldsymbol{t} = \mathrm{d}\boldsymbol{X}/\mathrm{d}s$ and $\mathrm{d}\boldsymbol{n}/\mathrm{d}s = \kappa\boldsymbol{t}$, yields the shrinkage rate over a material domain [8]:

$$\dot{s} = -\int \kappa^2 \mathrm{d}s \tag{29}$$

where $\dot{s}$ is the derivative of arc length, s, with respect to time. Since the characteristic length is known to scale with $t^{1/2}$ (see Section 4), it is appropriate to consider the rescaled arc length S, defined by

$$s = t^{1/2}S. \tag{30}$$

Substituting equation 30 into 29 and rearranging using $\kappa = K/t^{1/2}$ from Section 4, gives

$$\dot{S} = -\frac{1}{t}\int_0^S K^2 \mathrm{d}S - \frac{1}{2t}S. \tag{31}$$

The second term shows that even if the film element shrinkage stops i.e. $\dot{s} = 0$, then S will continue to decrease because of the overall expansion of the structure (scaling with $t^{1/2}$) induced by the shearing.

Clearly (on geometric grounds), both S and K can be expressed solely in terms of either r or θ. We choose to define $S = 0$ to be the symmetry point at $\theta = -\pi/4$, as identified in Section 4. Thus the similarity solution obtained in Section 4 (via equation 14 or equivalently equation 16), allows the movement of material points at any point on the film to be tracked by equation 31.

Since the film is being pulled at unit velocity, at time $t = t_0$, a material point is injected at a polar coordinate location $\tilde{r} = t_0$. For our asymptotic solution (which for computational simplicity is what we choose to analyse here) this corresponds to a θ value very close to (albeit not exactly) zero.

The movement of material points injected at $t_0 = 4$, 16 and 64 was calculated taking the asymptotic solution from Section 4, and considering points at the relevant initial location and tracking their motion in time. Results are shown in figure 10 and figure 11.

The behaviour of the angular location θ of material points as seen in figure 10 is straightforward. The period of time for which the angular position of a material point is nearly constant occurs when the point is on the near-straight section of the film (at $|\theta| \ll 1$, adjacent to the x-axis). Hence this behaviour is always observed for any material point with t_0 large enough that its initial location is indeed on the straight section of the film, and the duration of the period of nearly constant θ becomes longer with larger t_0. Eventually, typically at some time t on the order of t_0^2, the curved region of the film reaches the initially injected point and its polar angle θ begins to decrease. Eventually all material points approach $-\pi/4$ asymptotically at long times, at least in principle[6].

[6]Notice however that the system may require exceedingly long times for a material point to approach close to that final angle $-\pi/4$. Based on estimates given earlier, the time value of 10000 units needed in figure 10 for the point labelled as $t_0 = 16$ to migrate to within a few percent of $-\pi/4$ corresponds to 100 s of physical time. For curvature with a 'diffusivity' D of 10^{-4} m^2 s^{-1} (given earlier), this corresponds to an initially sharp-cornered

Figure 11 shows similar data but expressed in terms of the rescaled arc length coordinate S. This log-log plot suggests one straight line regime at early times, and a second straight line regime at long times[7]. At early times and for large S equation 31 is dominated by $\dot{S} \approx -S/(2t)$, since the integral $\lim_{S\to\infty} \int_0^S K^2 \mathrm{d}S$ remains finite. This gives a slope of $-\frac{1}{2}$ on the log-log plot and (as noted above) corresponds to S decreasing due solely to the $t^{1/2}$ overall length rescaling. At late times i.e. small S, the slope is steeper. Equation 31 becomes

$$\dot{S} \approx -\left(K_0^2 + \frac{1}{2}\right)\frac{S}{t} \tag{32}$$

where K_0 is the curvature at $S = 0$. Evaluating equation 13 at $\theta = -\pi/4$ gives $K_0 = -r_0/2$ where, as stated in Section 4, $r_0 \approx 1.0445$. Integration of equation 31 reveals a straight line on a log-log plot but now with a larger slope, $-\left(K_0^2 + \frac{1}{2}\right)$, agreeing with the second straight line regime seen in figure 11. Interestingly for the smallest t_0 value shown on figure 11 (i.e. $t_0 = 4$), the evolution follows the slope of this 'second' straight line region even at early times. The reason for this is made clear by comparing with figure 10: the $t_0 = 4$ material point never has exceedingly small values of $|\theta|$, thus it never finds itself on any long straight section of film adjacent to the x-axis. Rather it is injected onto an already curved section of film and its θ and S values evolve accordingly[8].

7 Conclusions

We have used the viscous froth model to describe a sheared foam film, with shear being introduced by dragging the film's end point at a constant velocity in a direction at right angles to the original film orientation. Although the system we consider is a highly idealised one, it

film becoming rounded over a curvature radius 0.1 m, which is longer than a typical film in a foam. In practice then, material points injected at either $t_0 = 16$ or $t_0 = 64$ case will not reach the neighbourhood of $\theta \sim -\pi/4$ on time or distance scales likely to be of interest in a real foam, although such material points could still see significant evolution of θ away from the initial $|\theta| \ll 1$ value.

[7]We note a similar caveat as previously i.e. for larger t_0 values, the times required to approach the second straight line region may be prohibitively large.

[8]The supposition that the $t_0 = 4$ material point is injected onto an already curved section of film is based here on the analysis of the long-time asymptotic solution of Section 4. Figure 5 however showed that at finite times, a flattened section of film can occur in the angular domain $-\pi/4 \leq \theta \leq 0$ *before* the long-time asymptotic film shape is actually achieved, and such a flattened section could affect the time evolution of θ or S as experienced by a material point. This however is beyond the scope of the analysis presented here.

nonetheless describes a generic process which is important in any sheared '2-dimensional' foam (i.e. in any system where a layer of bubbles is confined between upper and lower plates, and subjected to shear). In the foam system containing many bubbles, it is necessary to transport curvature along the entire length of a film so as to set a vertex in motion, leading eventually to a collision between two adjacent vertices. This initiates a so-called topological transformation that relaxes the energy in the foam as bubbles exchange neighbours. The first step in this chain of events is transport of curvature.

Our data show that after a time t, curvature is transported over a distance scaling like $t^{1/2}$, which underlines the diffusive nature of the transport inherent in the viscous froth model. The film end point however is moved at a constant velocity and hence its displacement grows linearly in time. It therefore migrates increasingly far away from the curved region as time evolves. The film end point becomes joined to the curved region of film by an almost straight segment which reorients itself (approximately exponentially in time) to align with the direction in which the film end point is being dragged. The film eventually approaches an asymptotic state corresponding to an infinite film containing an initial right angled corner, a system which admits a similarity solution whereby distances indeed scale like $t^{1/2}$ as expected.

Appendix

We have stated in the main text that curvature "diffuses" along films. The purpose of this section is to make this claim mathematically precise, and to indicate some of the physical consequences that this diffusion of curvature implies.

The idea of the diffusive nature of film curvature comes from the viscous froth model equation 3, ignoring pressure differences for simplicity. Using the notation from equation 3, and substituting $\kappa \boldsymbol{n} = -\mathrm{d}\boldsymbol{t}/\mathrm{d}s$ and $\boldsymbol{t} = \mathrm{d}\boldsymbol{X}/\mathrm{d}s$,

$$\left(\frac{\mathrm{d}\boldsymbol{X}}{\mathrm{d}t}\right)_{\Theta} = \frac{\mathrm{d}^2\boldsymbol{X}}{\mathrm{d}s^2} \tag{33}$$

which is analogous to Fick's law. There is however a slight complication – the left hand side of equation 33 is most naturally written in terms of material elements labelled by Θ while the

right hand side of equation 33 is most naturally written in terms of arc lengths s. Material elements do not however correspond precisely to arc length elements – indeed individual material elements tend to shrink as time goes on. Care must be exercised therefore, when manipulating equation 33 to derive a diffusion equation for curvature.

We proceed as follows. Since $\boldsymbol{X}$ can be considered as $\boldsymbol{X}(t, s(\Theta, t))$, we can derive a convective derivative as follows. First, we write

$$\left(\frac{\mathrm{d}\boldsymbol{X}}{\mathrm{d}t}\right)_{\Theta} = \left(\frac{\mathrm{d}\boldsymbol{X}}{\mathrm{d}t}\right)_{s} + \left(\frac{\mathrm{d}s}{\mathrm{d}t}\right)_{\Theta}\left(\frac{\mathrm{d}\boldsymbol{X}}{\mathrm{d}s}\right). \tag{34}$$

Substituting equation 29 (and treating s' as a dummy integration variable),

$$\left(\frac{\mathrm{d}\boldsymbol{X}}{\mathrm{d}t}\right)_{\Theta} = \left(\frac{\mathrm{d}\boldsymbol{X}}{\mathrm{d}t}\right)_{s} - \left(\frac{\mathrm{d}\boldsymbol{X}}{\mathrm{d}s}\right)\int_0^s \kappa^2 \mathrm{d}s' \tag{35}$$

and hence in general

$$\left(\frac{\mathrm{d}}{\mathrm{d}t}\right)_{\Theta} = \left(\frac{\mathrm{d}}{\mathrm{d}t}\right)_{s} - \left(\int_0^s \kappa^2 \mathrm{d}s'\right)\left(\frac{\mathrm{d}}{\mathrm{d}s}\right). \tag{36}$$

Applying $\boldsymbol{n}\cdot \mathrm{d}^2/\mathrm{d}s^2$ to each term of equation 35 and simplifying using equation 3 and the relationship $\mathrm{d}^2\boldsymbol{X}/\mathrm{d}s^2 = -\kappa\boldsymbol{n}$, gives

$$\begin{aligned}
\boldsymbol{n}\cdot\frac{\mathrm{d}^2}{\mathrm{d}s^2}\left(\frac{\mathrm{d}\boldsymbol{X}}{\mathrm{d}t}\right)_{\Theta} &= \boldsymbol{n}\cdot\frac{\mathrm{d}^2}{\mathrm{d}s^2}\left(\frac{\mathrm{d}\boldsymbol{X}}{\mathrm{d}t}\right)_{s} - \boldsymbol{n}\cdot\frac{\mathrm{d}^2}{\mathrm{d}s^2}\left(\left(\int_0^s \kappa^2\mathrm{d}s'\right)\frac{\mathrm{d}\boldsymbol{X}}{\mathrm{d}s}\right) \\
&= \boldsymbol{n}\cdot\left(\frac{\mathrm{d}}{\mathrm{d}t}\right)_{s}(-\kappa\boldsymbol{n}) - \boldsymbol{n}\cdot\left(\int_0^s \kappa^2\mathrm{d}s'\right)\frac{\mathrm{d}}{\mathrm{d}s}(-\kappa\boldsymbol{n}) \\
&\quad -\boldsymbol{n}\cdot 2\kappa\frac{\mathrm{d}\kappa}{\mathrm{d}s}\boldsymbol{t} - \boldsymbol{n}\cdot 2\kappa^2(-\kappa\boldsymbol{n}) \\
&= \boldsymbol{n}\cdot\left(\frac{\mathrm{d}(-\kappa\boldsymbol{n})}{\mathrm{d}t}\right)_{\Theta} + 2\kappa^3
\end{aligned} \tag{37}$$

where we have used the fact that $\boldsymbol{n}\cdot\boldsymbol{t}$ vanishes, we have also applied equation 36 to the vector $-\kappa\boldsymbol{n}$. Note in the above that

$$\left(\frac{\mathrm{d}(-\kappa\boldsymbol{n})}{\mathrm{d}t}\right)_{\Theta} = \left(\frac{\mathrm{d}}{\mathrm{d}t}\right)_{\Theta}\left(\frac{\mathrm{d}^2\boldsymbol{X}}{\mathrm{d}s^2}\right) \tag{38}$$

making it obvious that the operators $\mathrm{d}^2/\mathrm{d}s^2$ and $(\mathrm{d}/\mathrm{d}t)_{\Theta}$ do not commute. We can further simplify equation 37 by recognising that any derivative of $\boldsymbol{n}$ is necessarily orthogonal to $\boldsymbol{n}$ itself

and hence

$$\boldsymbol{n} \cdot \frac{\mathrm{d}^2}{\mathrm{d}s^2}\left(\frac{\mathrm{d}\boldsymbol{X}}{\mathrm{d}t}\right)_\Theta = -\left(\frac{\mathrm{d}\kappa}{\mathrm{d}t}\right)_\Theta + 2\kappa^3. \tag{39}$$

Applying $\boldsymbol{n} \cdot \mathrm{d}^2/\mathrm{d}s^2$ to the right hand side of equation 33, substituting $\mathrm{d}^2\boldsymbol{X}/\mathrm{d}s^2 = -\kappa\boldsymbol{n}$, and simplifying (using also the fact that $\mathrm{d}\boldsymbol{n}/\mathrm{d}s = \kappa\boldsymbol{t}$ and hence is orthogonal to $\boldsymbol{n}$),

$$\begin{aligned} \boldsymbol{n} \cdot \frac{\mathrm{d}^2}{\mathrm{d}s^2}\left(\frac{\mathrm{d}^2\boldsymbol{X}}{\mathrm{d}s^2}\right) &= \boldsymbol{n} \cdot \frac{\mathrm{d}^2\left(-\kappa\boldsymbol{n}\right)}{\mathrm{d}s^2} \\ &= -\frac{\mathrm{d}^2\kappa}{\mathrm{d}s^2} + \kappa^3. \end{aligned} \tag{40}$$

Equating 39 and 40 and simplifying gives

$$\left(\frac{\mathrm{d}\kappa}{\mathrm{d}t}\right)_\Theta = \frac{\mathrm{d}^2\kappa}{\mathrm{d}s^2} + \kappa^3, \tag{41}$$

which is the curvature diffusion equation that we seek.

Equation 41, like equation 33, is still parameterised in terms of material point and arc length coordinates, and takes an extremely compact and elegant form in those coordinates. When solving viscous froth problems however, one seldom parameterises in terms of either material points or arc lengths. Indeed the solution we obtained in Section 4 was described in terms of polar r *vs.* θ or θ *vs.* r coordinates. Once the system is solved in terms of polars, it is a straightforward geometry problem to obtain arc lengths. Meanwhile the analysis of Section 6 has shown how to recover material point positions. Thus arc lengths and material point locations are often determined after the film shape evolution has been solved, rather than as part of the technique for obtaining that evolution.

Despite the fact that we seldom solve problems using equation 41 directly, the equation remains useful conceptually. As a diffusion equation, it explains why curvature spreads over a distance of order square root of time as we showed in the analysis in the main text.

In a different physical context, it also explains why so-called grain growth problems behave differently from coarsening in a soap froth [13]. In both froth coarsening and grain growth – see [13] for details – certain domains grow whilst others shrink and disappear. Soap froth coarsening demands that domain boundaries are uniformly curved, according to the difference in gas pressure across the boundary. A shrinking bubble on the point of disappearance has a

much higher pressure than any of its neighbours with the result that curvature is nearly the same along each and every edge. A shrinking soap bubble therefore adopts a very regular shape. Grain growth models (which correspond to equation 41) permit much less regular shapes in shrinking domains. The time scale to diffuse curvature uniformly along a film (on the order of s^2 for a domain of length scale s) is similar to the time scale (again order s^2) for the domain to disappear altogether. Thus irregularities in shrinking domains persist in grain growth models all the way up to the disappearance of the grain. Grains are therefore far less regular than their soap froth counterparts.

Acknowledgements

GM and SC acknowledge financial support from FP7 IAPP project HYDROFRAC (PIAP-GA-2009-251475). PG also acknowledges support from FP7 IAPP project HYDROFRAC (PIAP-GA-2009-251475) which funded a visit to Aberystwyth. Part of this work also was carried out whilst PG was a Royal Academy of Engineering/Leverhulme Trust Senior Research Fellow and funding from the fellowship is gratefully acknowledged.

SC and PG acknowledge useful discussions with Prof. D. Weaire, and in particular Prof. Weaire's helpful insights at the 'Infoamal' Workshop on Foam Coarsening (Université Paris Diderot, 9th–11th January 2013), part-funded by CFCAM Ile-de-France.

References

[1] D. Weaire and S. Hutzler. *The Physics of Foams*. Oxford University Press, 1999.

[2] A. M. Kraynik. Foam flows. *Annu. Rev. Fluid Mech.*, 20:325–357, 1988.

[3] W. Drenckhan, S. J. Cox, G. Delaney, H. Holste, D. Weaire, and N. Kern. Rheology of ordered foams—on the way to discrete microfluidics. *Colloids Surf., A*, 263:52–64, 2005.

[4] T. E. Green, P. Grassia, L. Lue, and B. Embley. Viscous froth model for a bubble staircase structure under rapid applied shear: An analysis of fast flowing foam. *Colloids Surf., A*, 348:49–58, 2009.

[5] D. J. Durian. Foam mechanics at the bubble scale. *Phys. Rev. Lett.*, 75:4780–4783, 1995.

[6] T. Okuzono and K. Kawasaki. Intermittent flow behavior of random foams: A computer experiment on foam rheology. *Phys. Rev. E.*, 51:1246–1253, 1995.

[7] N. Kern, D Weaire, A. Martin, S. Hutzler, and S. J. Cox. Two-dimensional viscous froth model for foam dynamics. *Phys. Rev. E.*, 70:041411, 2004.

[8] T. E. Green, A. Bramley, L. Lue, and P. Grassia. Viscous froth lens. *Phys. Rev. E*, 74:051403, 2006.

[9] P. Grassia, G. Montes-Atenas, L. Lue, and T. Green. A foam film propagating in a confined geometry: Analysis via the viscous froth model. *Eur. Phys. J. E*, 25:39–49, 2008.

[10] S. J. Cox and G. Mishuris. Remarks on the accuracy of algorithms for motion by mean curvature in bounded domains. *J. Mechanics of Materials & Structures*, 4:1555–1572, 2009.

[11] S. J. Cox, D. Weaire, and G. Mishuris. The viscous froth model: Steady states and the high-velocity limit. *Proc. R. Soc. A*, 465:2391–2405, 2009.

[12] J. A. Glazier and D. Weaire. The kinetics of cellular patterns. *J. Phys., Condens. Matter*, 4:1867–1894, 1992.

[13] D. Weaire and S. McMurry. Some fundamentals of grain growth. *Solid State Phys.*, 50:1–36, 1996.

[14] S. J. Cox. A viscous froth model for dry foams in the Surface Evolver. *Colloids Surf., A*, 263:81–89, 2005. Special Issue: A collection of papers presented at the 5th European Conference on Foams, Emulsions and Applications, EUFOAM 2004, University of Marne-la-Vallée, Champs sur Marne (France), 5–8 July 2004, edited by M. Vignes-Adler, D. Weaire and R. Miller.

[15] F. Rouyer, S. Cohen-Addad, M. Vignes-Adler, and R. Höhler. Dynamics of yielding observed in a three-dimensional aqueous dry foam. *Phys. Rev. E*, 67:021405, 2003.

[16] H. M. Princen. Rheology of foams and highly concentrated emulsions. I. Elastic properties and yield stress of a cylindrical model system. *J. Colloid and Interf. Sci.*, 91:160–175, 1983.

[17] I. Cantat, N. Kern, and R. Delannay. Dissipation in foam flowing through narrow channels. *Europhys. Lett.*, 65:726–732, 2004.

[18] C. Raufaste, A. Foulon, and B. Dollet. Dissipation in quasi-two-dimensional flowing foams. *Phys. Fluids*, 21:053102, 2009.

[19] K. A. Brakke. *The Motion of a Surface by its Mean Curvature*. Princeton University Press, Princeton, NJ, 1978. Available from page http://www.susqu.edu/brakke.

[20] W. W. Mullins. Two-dimensional motion of idealized grain boundaries. *J. Appl. Phys.*, 27:900–904, 1956.

[21] K. A. Brakke. The Surface Evolver. *Experiment. Math.*, 1:141–165, 1992.

Table 1: Values of θ_f and A, corresponding to varying switch points at which the analytic approximation is implemented.

θ at switch	r at switch	θ_f	A
$-0.1\times\pi/2$	1.58	-0.012515	1.559
$-0.01\times\pi/2$	2.66	-0.000032	1.378
$-0.001\times\pi/2$	3.70	-0.000006	1.372
$-0.0001\times\pi/2$	4.57	-0.000006	1.372

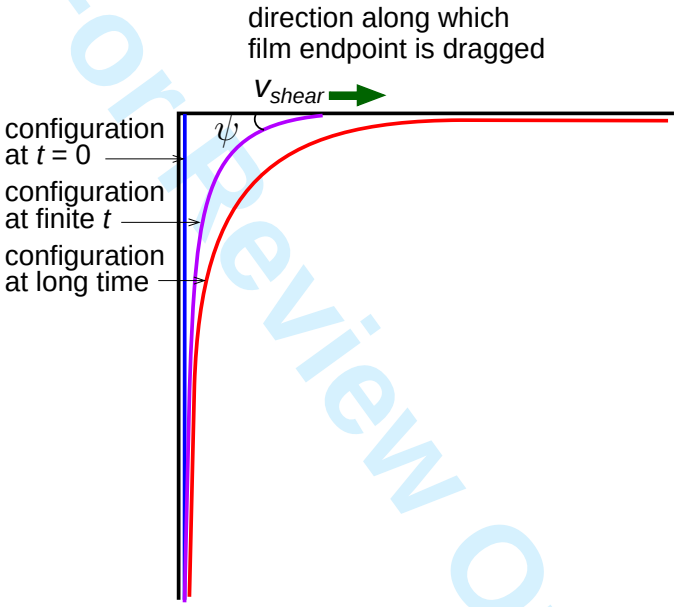

Figure 1: An initially semi-infinite film dragged perpendicularly to its initial orientation. The resulting curvature diffuses along the film, and the angle ψ which the film makes with the dragging direction decays.

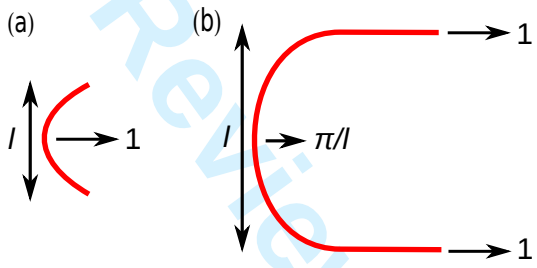

Figure 2: Different final states of the Mullins finger depending on the (dimensionless) end point separation l: (a) for $l < \pi$ the final state is a segment of a curve, and (b) for $l > \pi$ an arbitrarily long straight line section is observed, joining smoothly onto the curve.

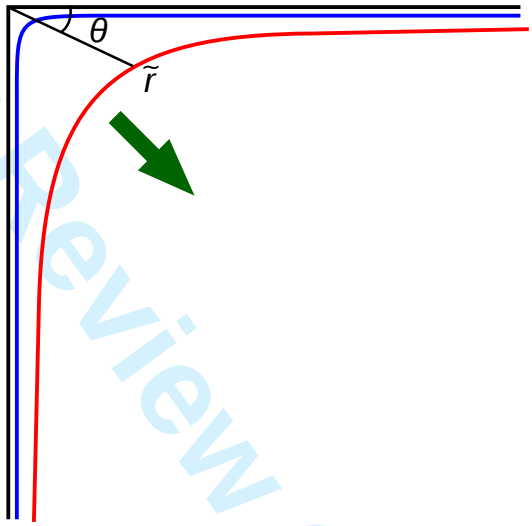

Figure 3: Sketch of the long time asymptotic solution of the sheared semi-infinite system, which corresponds to a similarity solution of an infinite film with a right angled corner at first, from which curvature diffuses away over time. Here θ is the angular position (in polar coordinates) and $\tilde{r}$ is the radial position which can be rescaled with respect to time t to obtain a rescaled similarity coordinate r.

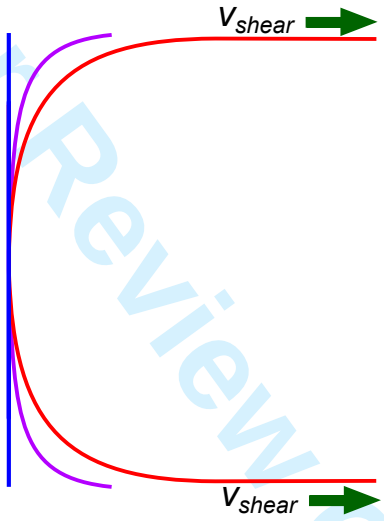

Figure 4: A sketch of the film studied numerically. As long as the straight (vertical) central section is present, the remaining curved region of the film is identical to the case of a semi-infinite film. For longer periods of time, the film itself needs to be longer to retain that straight central section.

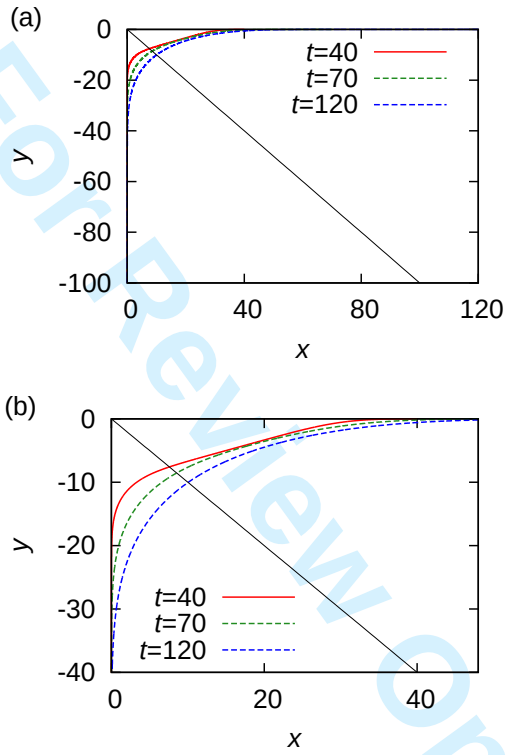

Figure 5: (a) Curve shapes computed by Surface Evolver for a film with $L = 200$ computed at times t of 40, 70 and 120. The end point at the top of the film has been displaced to position $x = t$ (although this is difficult to see on the scale of the plot). To guide the eye, the bisector of the quadrant at polar angle $\theta = -\pi/4$ is also indicated on the plot. (b) A zoomed version of the above.

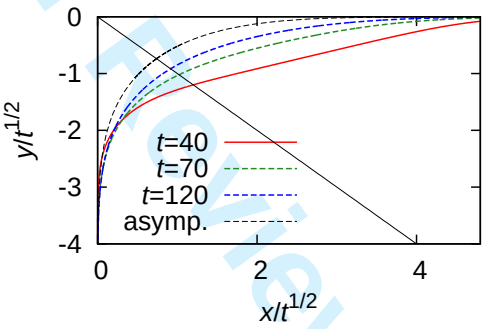

Figure 6: Curve shapes computed by Surface Evolver for a film with $L = 200$ computed at times t of 40, 70 and 120, but with distances scaled by $t^{1/2}$ (cf. figure 5). To guide the eye, the bisector of the quadrant $\theta = -\pi/4$ is also indicated. Moreover the asymptotic shape expected in the long time limit is shown (to be discussed in Section 4).

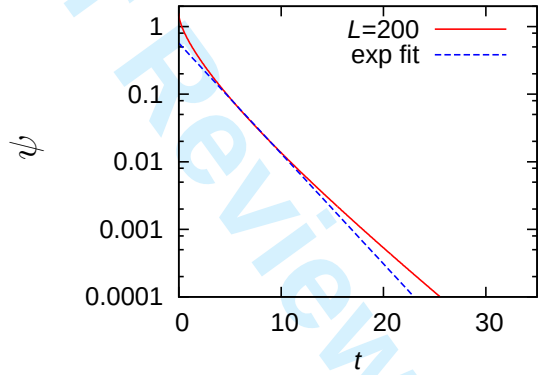

Figure 7: The angle ψ at which the dragged film meets the line along which its end point is dragged plotted as a function of time t. These data are for a film of length $L = 200$, although data for the case $L = 100$ would be indistinguishable. The decay of ψ is compared with an exponential fit, showing reasonable (albeit imperfect) agreement.

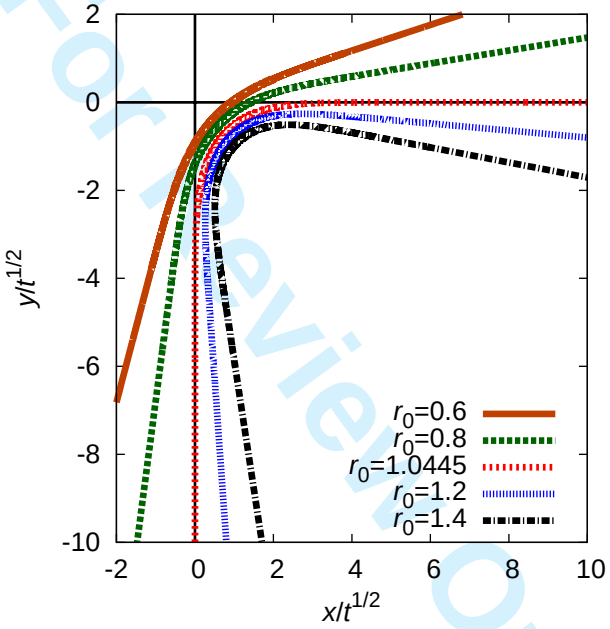

Figure 8: Solutions of film shape using varying values of r_0 (r at $\theta = -\pi/4$). Note that (as this is a similarity solution where the similarity variable is distance rescaled by the square root of time) the axes are labelled here as $x/t^{1/2}$ and $y/t^{1/2}$.

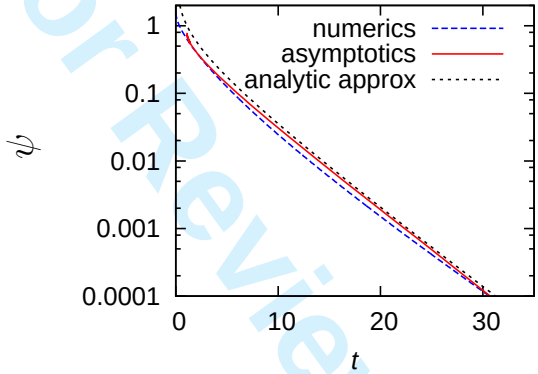

Figure 9: The plot shows the angle ψ between the vector tangent to the film and the x-axis at a given point on the film against time t. Numerical simulation data from Surface Evolver are shown (ψ being calculated at the film end point), and values are also shown from the asymptotic solution (ψ being calculated at the 'nominal' end point of the film, i.e. at $r = t^{1/2}$). An approximate analytic formula for ψ (equation 28 obtained from the asymptotic solution in the large t limit) is also shown. The complementary error function solution (equation 26) has not been shown here, as it is almost indistinguishable from the curve labelled 'asymptotics'.

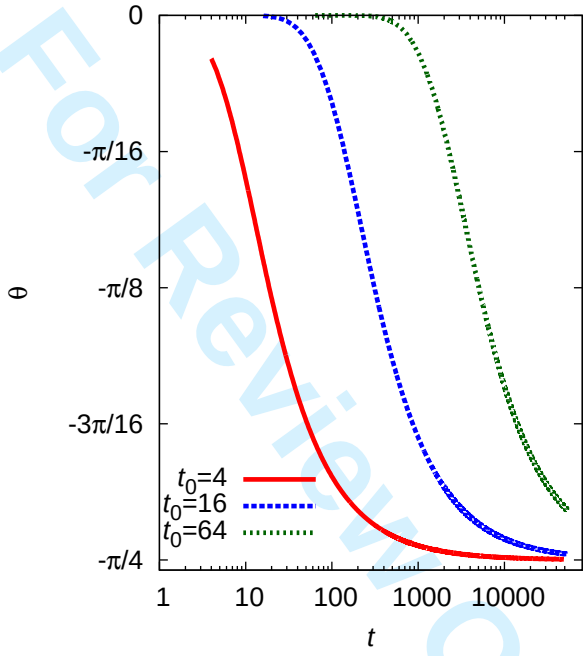

Figure 10: Plot of polar coordinate θ against t on a semi-log plot for material points injected onto the film at $t = t_0$. The initial period when θ is nearly constant (seen for larger t_0 values) is due to the material point migrating through the straight section of the film (located adjacent to the x-axis on a plot such as figure 6). As $t \to \infty$ any given material point eventually moves towards $\theta = -\pi/4$ (although, depending on t_0, this might happen only for exceedingly long times).

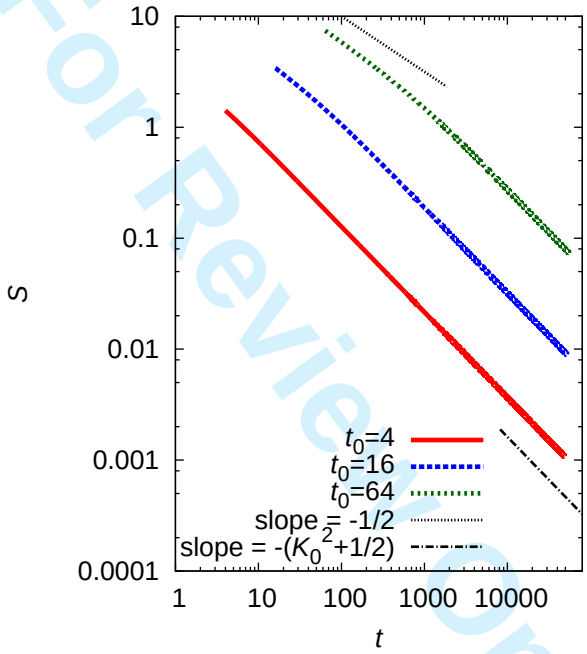

Figure 11: A log-log plot of S *vs.* t. Here t_0 is the time at which the material point is injected. A linear relationship (on these log-log axes) is observed at both high and low values of S, but with differing slopes in these different regimes.